EXPERIMENTAL CHARACTERIZATION OF STRESS CORROSION CRACKING SENSITIZATION IN AUSTENITIC STAINLESS STEEL USING NONLINEAR ULTRASONIC RAYLEIGH WAVES

A Thesis
Presented to
The Academic Faculty

by

Alexander J. Lakocy

In Partial Fulfillment
of the Requirements for the Degree
Master of Science in the
School of Civil and Environmental Engineering

Georgia Institute of Technology
December 2015

EXPERIMENTAL CHARACTERIZATION OF STRESS CORROSION CRACKING SENSITIZATION IN AUSTENITIC STAINLESS STEEL USING NONLINEAR ULTRASONIC RAYLEIGH WAVES

Approved by:

Professor Laurence J. Jacobs, Advisor
School of Civil and Environmental Engineering
Georgia Institute of Technology

Dr. Jin-Yeon Kim
School of Civil and Environmental Engineering
Georgia Institute of Technology

Professor Kimberly E. Kurtis
School of Civil and Environmental Engineering
Georgia Institute of Technology

Date Approved: 4 December 2015

ACKNOWLEDGEMENTS

I would like to first thank Prof. Laurence Jacobs, who advised my research. His endless energy, enthusiasm, and encouragement were instrumental in guiding my academic program. Prof. Jacobs' generosity is best characterized by his establishment of the pizza and coffee scholarship for needy graduate students, without which this thesis would not have been possible.

I also owe a great deal of acknowledgement to Prof. Kimberly Kurtis for many reasons, not the least of which were her recruitment efforts during my application process to Georgia Tech. In addition to her expert advising and teaching, she loaned me laboratory equipment and textbooks, which I promise to eventually return.

Further, I would like to thank Prof. Preet Singh, whose hospitality in allowing me to use his ovens to treat my specimens was greatly abused. His insights on the mechanisms of stress corrosion cracking and his extensive knowledge concerning chemical interrogation techniques were invaluable to this research.

A special thank you goes to Dr. Jin-Yeon Kim, whose genius is often underappreciated, but who always has an explanation, a solution, and a smile.

My deepest thanks to Prof. John Popovics at the University of Illinois for getting me started with research and providing much-needed advice throughout my undergraduate and graduate studies.

To Joe Wall at the Electric Power Research Institute — thank you for your support and expertise. Your balanced optimism provided me with much-needed encouragement over the past two years.

Thanks to my lab-mates: David Torello, who knows all there is to know about electromagnetic interference and, more importantly, where all the best coffee shops

are; Gun Kim, concrete degradation expert and the best road-trip partner anyone could ask for; Katie Scott, whose work ethic and perseverence are an inspiration; Matthias Uhrig, the smartest and most talented athlete I will ever meet; Tobias Oberhardt, whose German language teaching skills are surpassed only by his sense of humor; and Aulon Bajrami, whose sleep patterns defy any logical explanation. I especially want to thank Sara Palagyi, a quick learner and a fantastic co-worker, whose efforts in the lab are greatly appreciated. All of you make lab work seem "fun", and I am grateful for your support.

I would further like to acknowledge financial support from the National Science Foundation through the Graduate Research Fellowship Program.

Finally, a great big thank you for my family and friends, without whom I would have given up long ago.

TABLE OF CONTENTS

LIST OF TABLES

LIST OF FIGURES

SUMMARY

This thesis examines the use of nonlinear ultrasound to evaluate sensitization, a precursor to stress corrosion cracking in austenitic stainless steel. Ultrasonic Rayleigh surface waves are generated on a specimen; as these waves pass through sensitized material, second harmonic generation (SHG) increases. In austenitic stainless steel with oven-induced sensitization, this increase is due only to the formation of chromium carbide precipitates, key products of the sensitization process. Weld-induced sensitization specimens demonstrate additional increases in SHG, likely caused by increased residual stress and dislocation density as a result of uneven heating. Experimental data are used to calculate the acoustic nonlinearity parameter, which provides a single value directly related to the quantity of micro- and nano-scale damage present within any given sample. Using this procedure, the effects of weld- and oven-induced sensitization are compared. Results demonstrate the feasibility of using nonlinear Rayleigh waves to detect and monitor stress corrosion susceptibility of welded material.

CHAPTER I

INTRODUCTION

1.1 Motivation and Objectives

The aging and deterioration of structural systems in the United States has become a critical public safety issue, as much of the American infrastructure is either rapidly approaching or has already surpassed its original design life[2]. In the interest of responsibly and economically maintaining this infrastructure, there is a need for techniques which have the capability to quantify both the current state and the remaining useful life of structural components without sacrificing operational objectives. This need is particularly apparent in the nuclear and petrochemical industries, where appropriate quantitative nondestructive evaluation (NDE) of primary and utility piping systems can help to avoid costly facility shutdowns and mitigate the risk of catastrophic failure[9].

Transport of harsh chemicals and other fluids via utility lines exposes pipe material to corrosion risk. Knowing this, many industrial facilities specify type 304 stainless steel, a material which is far more ductile and corrosion resistant than carbon steel, for use in their piping systems. However, the additional corrosion resistance of this austenitic stainless steel can be unintentionally reduced through a thermal process called sensitization, which often occurs adjacent to through-thickness welds[20]. After sensitization, 304 stainless steel becomes susceptible to intergranular stress corrosion cracking, a degradation mechanism characterized by significant reductions in both ultimate tensile strength and fracture toughness. If allowed to progress, this process can lead to early brittle failure of key components of industrial systems.

There is not an immediately obvious solution to this problem. Replacement of 304

stainless steel with a different material, such as the low-carbon 304L stainless steel, may take decades to complete, and would be prohibitively expensive. Other solutions, such as wrapping all potential hazardous regions with additional material, face similar issues — applying a fix to locations where it is not necessary is both expensive and wasteful. Post-weld annealing presents logistical challenges for field-welded structures and does not always adequately passivate sensitized material. A more economical and sustainable solution is the use of a non-destructive metric to quantitatively assess the risk of stress corrosion. This solution allows users to determine and monitor the material damage state at any locations and repair or replace only the material deemed to be at or above an acceptable risk level. The only requirement is an appropriate method which has been shown to be sensitive to stress corrosion cracking indicators. This thesis will examine the use of nonlinear ultrasound (NLU) for the purpose of quantitatively detecting sensitization in austenitic stainless steel caused by uniform (oven) and non-uniform (weld) heating. The objectives of this research are as follows:

Objective 1: Determine whether nonlinear ultrasound using Rayleigh waves is sensitive to both oven- and weld-induced sensitization in austenitic stainless steel specimens. This objective requires the use of nonlinear ultrasound on three different specimens: First, base (undamaged) material which has not undergone sensitization of any kind; second, material which has been sensitized using a uniform (oven) heat treatment; third, material which has been sensitized through a welding process. While the oven-induced sensitization specimens are expected to provide a more consistent set of measurements, the welded material provides far more realistic treatment and is more useful for practical purposes. Most sensitized material in the industrial world results from welding, not from uniform heating.

Objective 2: Quantify contributions to nonlinearity from precipitate formation and dislocation density using the acoustic nonlinearity parameter

β. NLU has previously demonstrated sensitivity to many factors in a variety of metallic and non-metallic materials. While material which has undergone oven-induced sensitization is likely to only have been affected by the formation of precipitates, it is anticipated that weld-induced sensitization specimens will see additional nonlinear effects caused by the welding process. This objective is to identify and quantify these other effects, which may include residual stress and dislocation density as a result of uneven heating. This is done using previous work in NLU theory. Models have been previously examined which approximate the effects of each of these mechanisms. Comparison of these estimates to results from experimentation provides a basis for quantification of the many microstructural changes experienced by welded specimens.

1.2 Structure of Thesis

This thesis is organized as follows. The first chapter introduces the problems associated with stress corrosion cracking and sensitization in austenitic stainless steels, and also provides the objectives of the research performed to examine these issues. Chapter 2 discusses the mechanisms for initiation and propagation of intergranular stress corrosion cracking, and identifies key effects of the process which may allow the use of NLU to examine or monitor such damage. In Chapter 3, the theory behind NLU and its potential for application to the current research are examined. The methods used to measure nonlinearity experimentally are described in Chapter 4. Results are presented and discussed for measurement of oven- and weld-induced sensitization in Chapters 5 and 6, respectively. Chapter 7 outlines conclusions from this work and Chapter 8 discusses future research to be performed.

CHAPTER II

STRESS CORROSION CRACKING

Stress Corrosion Cracking (SCC) is a degradation mechanism characterized by microcrack formation at low stress levels within metallic materials. This phenomenon is caused by the combination of a corrosive environment and a local tensile stress which together can lead to significant, lasting reductions in both mechanical strength and fracture toughness[5]. These two conditions are present in many applications, including industrial environments where harsh chemicals may be present, as well as coastal environments where warm, humid, mildly corrosive atmospheric conditions can provide a forcing for SCC. Since the formation of microcracks can occur at very small length scales, residual stress from a weld or other thermal treatment can often provide the local tensile stress necessary for SCC initiation, even if the bulk applied stress is far beneath the material yield strength.

2.1 304 Stainless Steel

Recognition that SCC can occur in a multitude of locations and environments often leads designers to specify materials such as type 304 stainless steel for applications where corrosion resistance is required. Table 1 shows the composition of type 304 stainless steel, which contains 18% Chromium and 8% Nickel by weight. Both of these elements contribute to the relatively high overall corrosion resistance of the material, which greatly exceeds that of typical structural carbon steel. Widespread use of 304 stainless steel in applications ranging from nuclear power systems to commercial food preparation has resulted in resilient structures and components which are generally capable of withstanding moderately corrosive environments.

Table 1: Composition of AISI Types 304 and 304L Stainless Steels[18]

Element	**% wt. 304**	**% wt. 304L**
Fe	66 - 74%	65 - 74%
Cr	18 - 20%	18 - 20%
Ni	8.0 - 11%	8.0 - 12%
Mn	<2.0%	<2.0%
Si	<1.0%	<1.0%
C	<0.08%	<0.03%
P	<0.045%	<0.045%
S	<0.03%	<0.03%

2.2 Sensitization

As shown in Table 1, type 304 stainless steel contains up to 0.08% carbon, an amount which generally exceeds the solubility of carbon in austenite at normal operating temperatures. When heated between approximately 450 - 850°C, the diffusion rate of small carbon atoms within the material increases (while the rate for much larger chromium atoms remains low), and a lack of solid solution equilibrium drives these carbon atoms out of the bulk material and into the boundaries between adjacent grains. Here, the migrating carbon reacts with chromium to form chromium carbide precipitates ($Cr_{23}C_6$). Chromium atoms provide the majority of corrosion resistance to stainless steels, and the formation of these precipitates reduces the concentration of chromium near grain boundaries. The result of this phenomenon, called "sensitization", is a network of chromium-depleted regions where resistance to corrosion is reduced[5]. Figure 1 shows two micrographs of the same specimen before and after sensitization.

Subsequent exposure of sensitized regions to corrosive environments leads to intergranular stress corrosion cracking, a series of microcracks which develop around the edges of austenite grains within stainless steel. In the presence of an applied tensile stress, these microcracks rapidly coalesce to form larger macrocracks, which

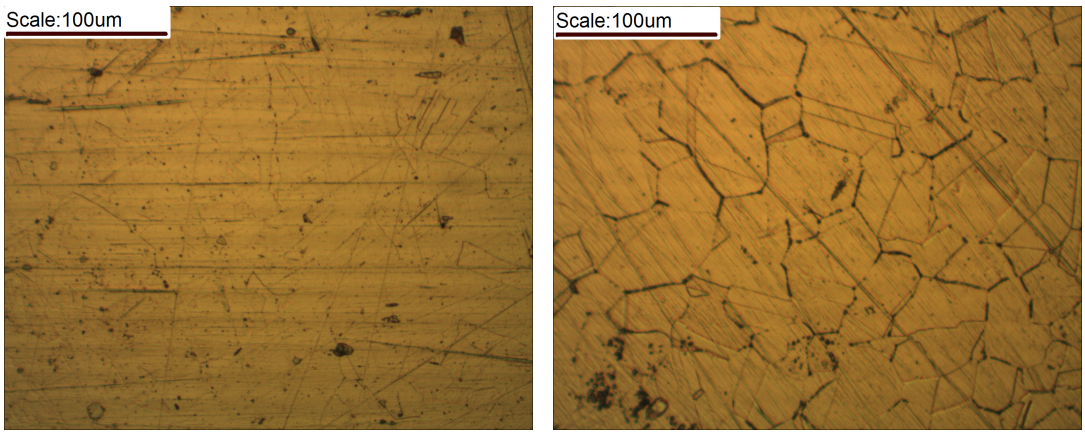

Figure 1: Comparison of untreated (left) and sensitized (right) microstructures

can greatly reduce the ultimate tensile strength and ductility of austenitic stainless steels.

In general, sensitization of 304 stainless steel results from one of two sources — uniform heating or welding. Typically, heating uniformly produces an even distribution of precipitates with few secondary effects. On the other hand, the intense thermal effects from welding can include local variation in precipitate size and density, grain size, and residual stresses. Type 304 stainless steel is rarely operational at uniform sensitization temperatures, meaning that most stress corrosion cracking occurs as a result of welding. Empirical observations indicate that weld-induced sensitization (and subsequent stress corrosion cracking) often occurs in the heat-affected zone (HAZ) of field-welded pipes which operate in mildly corrosive environments[9]. This means that the ability to detect weld-induced sensitization is key to the development of non-destructive evaluation techniques for stress corrosion cracking susceptibility. Without this ability, field testing for sensitization becomes far more difficult.

Formation of chromium carbide precipitates at grain boundaries of austenitic stainless steel provides the vital link between sensitization and detection. The formation of such precipitates changes the nature of the localized stress-strain relationship in the surrounding material, which has a significant effect on the measured material

nonlinearity — a topic which will be discussed in greater detail in Chapter 3.

2.3 Prevention

The stress corrosion cracking mechanism relies on a combination of several factors: applied stress, corrosive environment, and susceptible material. In general, removal of any of these three factors will result in a resilient system which should not experience stress corrosion cracking.

2.3.1 Change operating environment

One method to prevent stress corrosion cracking involves modifying the environment in which the material operates — generally either by reducing the concentration of chemical aggressors or by reducing the operating temperature in order to slow the corrosion process. Although this is the most effective method, altering the environment in which the material operates is often unfeasible, if not completely counter to the purpose of specifying corrosion-resistant material in the first place.

2.3.2 Use different materials

As discussed in Section 2.2, stress corrosion cracking will only proceed in austenitic stainless steels if the excess (insoluble) carbon within the material migrates to the grain boundaries and reacts with chromium ions to form chromium carbide precipitates. One way to prevent this is to eliminate this excess carbon from the material, preventing sensitization. As shown in Table 1, type 304L stainless steel is composed of less than 0.03% carbon, meaning that it is less likely to experience sensitization than is type 304. The use of 304L stainless steel has become far more prevalent as many fabricators recognize the advantages of material which will not sensitize. Indeed, it is difficult today in the United States to secure traditional 304 stainless steel — even material labeled as such by the manufacturer often contains less than 0.03% carbon, meaning that it technically qualifies as both type 304 and type 304L. However, the

majority of pipe material in existing industrial and petrochemical facilities is still constructed of type 304 stainless steel, and replacement with the more resilient 304L would be prohibitively expensive and wasteful.

2.3.3 Perform post-weld heat treatment

Another way to prevent stress corrosion cracking is through a post-weld heat treatment. Some research has shown that solution annealing followed by a water quench significantly increases the repassivation energy of stainless steel, restoring corrosion resistance to affected material[1]. This technique may be possible for some small structures, but is not feasible for pipeline systems, where achieving the required annealing temperature of 1050°C is impractical.

2.3.4 Use additional material

While the growth of microcracks caused by sensitization and subsequent stress corrosion cracking may be the underlying cause of material failure, it is possible to prevent catastrophic failure in high-risk regions by increasing the cross-sectional area of the structure in question. This can be done, for example in welded pipes, by wrapping with additional material — particularly through the use of bolted "collars" (as further welding would likely create more sensitized regions, exacerbating the issue). Without knowing where the material has been sensitized, however, this solution is once again prohibitively expensive.

2.3.5 Measurement and monitoring

It is clear that, in order to prescribe a solution to fix material affected by stress corrosion cracking, the regions that have been sensitized must first be located. The missing link in this operation is an evaluation method capable of detecting sensitized microstructures without destroying the host material. Such a method could be used a single time to detect sensitization, or else employ structural health monitoring

techniques to provide a consistent measure of the remaining structural capacity of the desired component (for example, by constantly measuring the amplitude of response to a stress wave, which would locate growing cracks). Chapter 3 will discuss the use of nonlinear ultrasound for this purpose.

CHAPTER III

NONLINEAR ULTRASOUND

Linear ultrasonic methods have been used extensively in the field of NDE since the 1970s. Originally developed for use in the medical industry, they were discovered to provide a system of simple and reliable measurements for detection and location of large subsurface flaws and defects. In particular, linear ultrasound excelled at identifying voids within welds, and is still used extensively for this purpose today. Ultrasound involves the use of an acoustic wave at frequencies above the limit of human hearing, and "linear" ultrasound refers to the measurement of linear properties of these waves. These properties include attenuation (how rapidly a signal deteriorates as it passes through a material), wave speed (a function of the density and elastic material properties), and signal response time (for subsurface flaw detection).

While linear ultrasonic methods are extremely useful for many applications, they are limited to detection of flaws and defects with dimensions on the order of the signal wavelength used to interrogate the material. Nonlinear ultrasound, on the other hand, is sensitive to defects orders of magnitude smaller than the wavelength, making it a good candidate for quantifying micro- and nano-scale damage within the bulk of a material. Previous studies have indicated that nonlinear ultrasound is more sensitive than linear methods to microstructural changes caused by a wide variety of damage mechanisms. This chapter demonstrates the evolution of the acoustic nonlinearity parameter, β, a quantity which will be used to evaluate the progression of sensitization in stainless steel specimens.

3.1 Wave Propagation

This derivation is in accordance with Bedford[4]. Equation (1) describes the conservation of linear momentum:

$$\int_V \rho \ddot{\boldsymbol{u}} \ dV = \int_S \boldsymbol{t} dS + \int_V \boldsymbol{b} dV \tag{1}$$

Here, $\boldsymbol{t}$ and $\boldsymbol{b}$ represent the surface traction and body force applied to a closed body, whose volume and surface are given by V and S, respectively. The value $\ddot{\boldsymbol{u}}$ represents the second derivative of displacement $\boldsymbol{u}$ with respect to time. Cauchy's stress definition is as follows:

$$t_i = n_j \sigma_{ij} \tag{2}$$

Applying Gauss' theorem and writing in index notation using Cauchy's stress gives:

$$\int_V \rho \frac{\partial^2 u_i}{\partial t^2} dV = \int_V \partial_j \sigma_{ij} dV + \int_V b_i dV \tag{3}$$

Equation (3) must hold for any volume V. Therefore, if the volume is assumed continuous, the **equation of balance of linear momentum** is obtained:

$$\rho \frac{\partial^2 u_i}{\partial t^2} = \partial_j \sigma_{ij} + b_i \tag{4}$$

In elastic materials, the stress at any point depends only on the strain at that point. For linear elastic materials with zero inital strain, this relationship is characterized by Equation (5), where σ is stress, C is an elastic constant, and ϵ represents strain:

$$\sigma_{km} = C_{kmij} \epsilon_{ij} \tag{5}$$

Solving for strain gives:

$$\epsilon_{ij} = h_{ijkm} \sigma_{km} \tag{6}$$

Here, h_{ijkm} are constants. Applying a uniform shear stress τ_0 such that $\sigma_{12} = \tau_0$ gives strain component ϵ_{11} as:

$$\epsilon_{11} = (h_{1112} + h_{1121}) \tau_0 \tag{7}$$

Application of the opposite shear stress $-\tau_0$ in a coordinate system where the x_2 direction is reversed, but the x_1 direction remains the same results in:

$$\epsilon_{11} = -(h_{1112} + h_{1121})\tau_0 \tag{8}$$

Since the strain ϵ_{11} in Equations (7) and (8) must be the same, it follows that $h_{1112} + h_{1121} = 0$. Extending this argument to additional dimensions demonstrates the **isotropic, linear-elastic stress-strain relationship**:

$$\sigma_{ij} = \lambda\delta_{ij}\epsilon_{kk} + 2\mu\epsilon_{ij} \tag{9}$$

Here, δ_{km} is the Kronecker delta, while λ and μ are the first and second Lamé constants. Equation (9) can also be written in terms of the more commonly used Young's modulus E and Poisson's ratio ν, which are defined below:

$$\lambda = \frac{E\nu}{(1+\nu)(1-2\nu)} \tag{10}$$

$$\mu = \frac{E}{2(1+\nu)} \tag{11}$$

From the definition of strain, it is apparent that the **linear strain tensor** is given by:

$$\epsilon_{ij} = \frac{1}{2}(\frac{\partial u_i}{\partial x_j} + \frac{\partial u_j}{\partial x_i}) \tag{12}$$

For the purposes of wave propagation, body force contributions in the conservation of momentum equation are typically negligible ($b_i = 0$). Further, spatial variation of the Lamé constants are neglected in homogeneous materials ($\nabla\lambda = 0$ and $\nabla\mu = 0$). Combining the stress-strain relationship with the conservation of momentum equation yields the following vector partial differential equation:

$$\rho\frac{\partial^2 \boldsymbol{u}}{\partial t^2} = (\lambda + \mu)\nabla(\nabla \cdot \boldsymbol{u}) + \mu\nabla^2\boldsymbol{u} \tag{13}$$

Using the vector Laplacian identity $\nabla^2\boldsymbol{a} = \nabla\nabla \cdot \boldsymbol{a} - \nabla \times \nabla \times \boldsymbol{a}$, Equation (13) can be re-written as shown below:

$$\rho\frac{\partial^2 \boldsymbol{u}}{\partial t^2} = (\lambda + 2\mu)\nabla(\nabla \cdot \boldsymbol{u}) - \mu\nabla \times \nabla\boldsymbol{u} \tag{14}$$

The Helmholtz decomposition represents a displacement field in terms of the sum of the gradient of a scalar potential ϕ and the curl of a vector potential $\boldsymbol{\psi}$:

$$\boldsymbol{u} = \nabla\phi + \nabla \times \boldsymbol{\psi} \tag{15}$$

Substituting Equation (14) into Equation (15) gives:

$$\nabla\left[\rho\frac{\partial^2\phi}{\partial t^2} - (\lambda + 2\mu)\nabla^2\phi\right] + \nabla \times \left[\rho\frac{\partial^2\boldsymbol{\psi}}{\partial t^2} - \mu\nabla^2\boldsymbol{\psi}\right] = 0 \tag{16}$$

Equation (16) is satisfied when the potentials ϕ and $\boldsymbol{\psi}$ satisfy the equations:

$$\frac{\partial^2\phi}{\partial t^2} = \alpha^2\nabla^2\phi, \quad \alpha = \left(\frac{\lambda + 2\mu}{\rho}\right)^{1/2} \tag{17}$$

$$\frac{\partial^2\boldsymbol{\psi}}{\partial t^2} = \beta^2\nabla^2\boldsymbol{\psi}, \quad \beta = \left(\frac{\mu}{\rho}\right)^{1/2} \tag{18}$$

These two uncoupled equations represent longitudinal (P) and shear (S) waves, respectively. The quantities α and β here express the respective phase velocities of these waves, and will be referred to as c_D and c_S for the remainder of this paper in order to avoid confusion with other symbols.

3.2 Acoustic Nonlinearity Parameter

For a wave traveling through an isotropic material with quadratic nonlinearity, the equation of motion can be written as:

$$\rho\frac{\partial^2 u}{\partial t^2} = \frac{\partial\sigma_{11}}{\partial x_1} \tag{19}$$

The constitutive equation for such a material is then expressed according to Equation (20):

$$\sigma_{11} = E_1(\frac{\partial u}{\partial x_1}) + \frac{1}{2}E_2(\frac{\partial u}{\partial x_1})^2 + ... \tag{20}$$

where E_1 and E_2 are the according material elastic constants. The corresponding wave equation is then:

$$\frac{\partial^2 u}{\partial x_1^2} = c^2 \left[1 - \beta \frac{\partial u}{\partial x_1}\right] \frac{\partial^2 u}{\partial x_1^2} \tag{21}$$

Here, β is the acoustic nonlinearity parameter, and is a function of the material elastic constants. The solution to Equation (21) can be written as follows:

$$u = A_1 sin(\kappa x_1 - \omega t) + A_2 sin(2\kappa x_1 - 2\omega t) + ... \tag{22}$$

where A_1 is the amplitude of the propagating wave with fundamental frequency $f = \frac{\omega}{2\pi}$, and A_2 is the amplitude of the wave's second harmonic component. In the absence of effects from scattering, attenuation, and diffraction, this second harmonic amplitude has been shown to satisfy Equation (23).

$$A_2 = \frac{\beta A_1^2 x \kappa^2}{8} \tag{23}$$

The acoustic nonlinearity parameter, β, can be isolated from Equation (23) to give the following relation:

$$\beta = \frac{8A_2}{A_1^2 x \kappa^2} \tag{24}$$

Using Equation (24), the acoustic nonlinearity parameter can be computed by measuring the fundamental and second harmonic amplitudes A_1 and A_2 of the wave, knowing the propagation distance x and the wavenumber κ. This relation, derived for longitudinal waves, holds similarly for Rayleigh waves, which will be examined in Section 3.4[21]. In general, however, the relative acoustic nonlinearity parameter, β', is used for experimentation, as piezoelectric transducers are not capable of directly measuring absolute wave amplitudes:

$$\beta' = \frac{A_2}{A_1^2 x} \propto \beta \tag{25}$$

where A_1 and A_2 are the fundamental and second harmonic amplitudes output by the piezoelectric transducer. The relative acoustic nonlinearity parameter will be examined in greater detail in Section 4.3.

3.3 Longitudinal Nonlinear Ultrasound

The acoustic nonlinearity parameter β is affected by two factors: the crystal structure of the material under investigation and the presence of localized strain. While the crystal structure remains unchanged for many applications, there are a number of microstructural effects which impose a residual strain field, and previous work has demonstrated the capability of nonlinear ultrasound using longitudinal waves to detect these various effects.

3.3.1 Dislocation density

The contribution of dislocations to the acoustic nonlinearity parameter was first recognized by Hikata and further examined by Cantrell[12][6]. The mechanism for second harmonic generation exists through the bowing of dislocation segments between two pinning points with a small initial stress σ_1. Each individual dislocation generates a miniscule quantity of energy in higher harmonic frequencies; however, in a material with many such dislocations, the effect is great enough to be significant.

An example of the effect of dislocations on material nonlinearity is demonstrated in fatigue specimens. Cantrell and Yost first proposed a formulation for the nonlinearity contribution from this effect in 2001[7]. This model estimated an increase of roughly 210% in the nonlinearity parameter for a high cycle fatigue, Al-2024-T4 specimen. Subsequent experiments demonstrated a 200% increase in β' over 100 kilo-cycles, indicating good agreement with the model.

Dislocation density is also impacted by the quenching process in martensitic steels. Avoiding significant changes in crystal structure, Hurley et al. performed nonlinear ultrasound on three different quenched steel materials to examine the relationship

between dislocation density, which is known to increase with carbon content, and the relative acoustic nonlinearity parameter, β'[13]. By roughly tripling the dislocation density, an increase of 11% in β' was observed.

3.3.2 Precipitate formation and growth

Precipitate formation and growth contribute to the localized strain field in a material. Consider a uniform, homogeneous material with a single interstitial precipitate. If the characteristics of the precipitate differ from those of the host material, the presence of this precipitate alters the interatomic spacing of the matrix and thus imposes localized residual strain on the crystal lattice structure. The larger the difference, or "misfit" between the precipitate and matrix, the greater the residual strain, and this leads to higher second harmonic generation. The precipitate-matrix contribution was first formulated by Cantrell and Zhang in 1998[8]. However, they determined that the precipitates themselves contribute relatively little to the acoustic nonlinearity; rather, the greatest effect is seen when precipitate formation and growth interact with dislocations. Formation and growth of large precipitates can impose strain on dislocation segments and even nucleate misfit dislocations themselves. Both of these actions cause much greater increases in the measured material nonlinearity.

The most common experiments demonstrating formation of precipitates relate to thermal aging. Cantrell and Yost experimentally measured the relative acoustic nonlinearity parameter for 2024 aluminum during artificial aging from the T4 to the T6 temper. It was shown that for precipitates which form through phase transformation (not solute migration), precipitate nucleation decreases material nonlinearity, while precipitate growth causes an increase in nonlinearity. During the overall aging process, a 10% net increase in β' was observed, indicating that the decrease from precipitate formation may have outweighed the increase caused by precipitate growth.

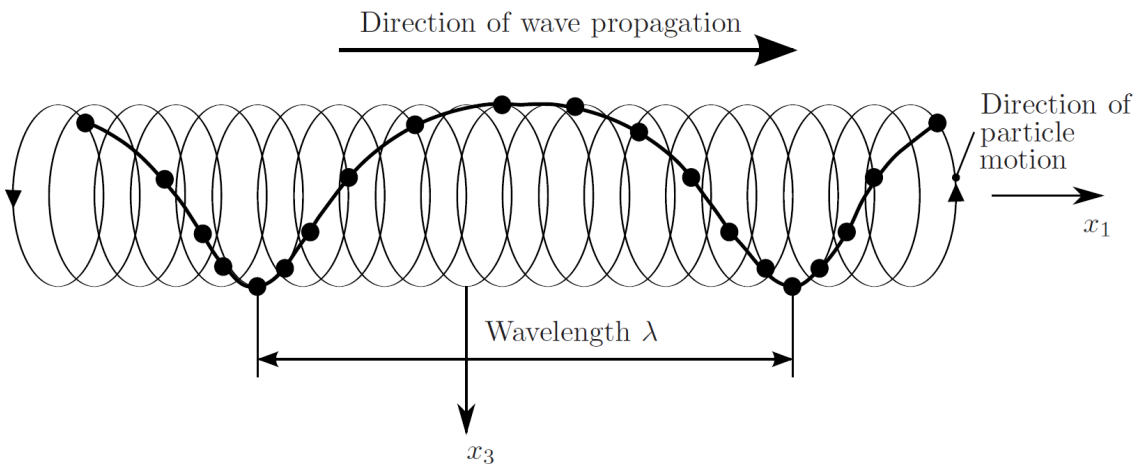

Figure 2: Schematic diagram showing elliptical path of Rayleigh Surface Waves[16]

These results indicate the sensitivity of longitudinal nonlinear ultrasound to degradation mechanisms which impose localized strain fields on material in the presence of dislocations. Section 3.4 discusses the use of nonlinear Rayleigh waves as a more practical method to examine these same mechanisms.

3.4 Rayleigh Surface Waves

Longitudinal (P) waves involve particle displacement along the direction of wave propagation, while shear (S) waves propagate normal to the particle displacement direction. First theorized by Lord Rayleigh in 1885, Rayleigh surface waves are actually a combination of both shear and longitudinal waves, meaning that particles in a Rayleigh wave follow elliptical paths of motion, as shown in Figure 2. Rayleigh waves offer several important advantages over their longitudinal counterparts for use with nonlinear ultrasound.

Rayleigh surface waves propagate along the surface of a material, generally penetrating only on the order of one wavelength into the thickness of the material. This means that measurements made using these waves are highly sensitive to surface defects — a useful characteristic for many applications where damage is concentrated near the outer surface. This property also means that, unlike with longitudinal waves,

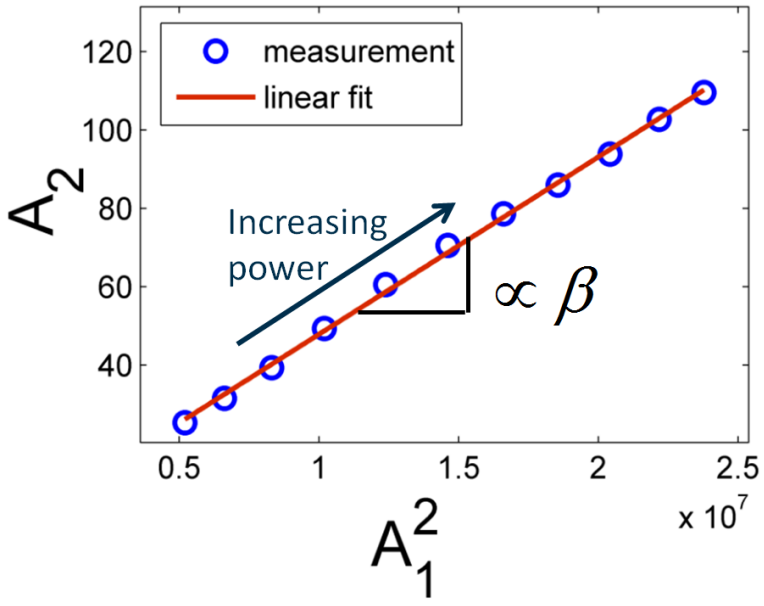

Figure 3: Plot showing data points obtained from NLU using longitudinal waves with increasing power[22]

nonlinear ultrasound using Rayleigh waves requires access to only one side of the structure or component under investigation. For pipe investigations, this is a key advantage, as no NDE method for piping systems can truly be "non-destructive" if it requires access to an interior pipe wall.

Computation of the relative acoustic nonlinearity parameter β' in accordance with Section 3.2 using longitudinal waves requires that the input power be manipulated. This manipulation produces the various data points for a linear fit of A_2 versus A_1^2, which is proportional to β' (see Figure 3. However, by changing the input power, there is also a change in the nonlinearity generated by the system. The transducers, function generator, and amplifiers each change their output slightly with changing input power, and any component nonlinearity is not easily distinguished from second harmonic generation within the material itself, as shown in Figure 4.

The use of Rayleigh waves eliminates this difficulty. The inverse of the propagation distance, $1/x$, is proportional to the nonlinearity parameter. Therefore, instead of fitting A_2 versus A_1^2, the quantity A_2/A_1^2 can be plotted against the propagation

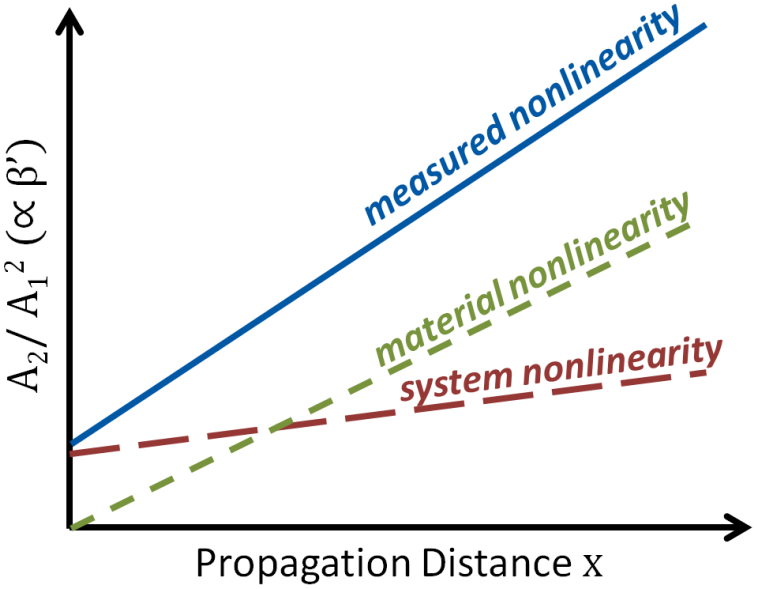

Figure 4: Simplistic diagram indicating the contribution of system nonlinearity to measured nonlinearity when varying input power[22]

distance x. By changing this propagation distance (along the surface of the material under investigation), multiple data points can be gathered without changing the input power, and the system nonlinearity will thus remain unchanged throughout the set of measurements. The slope of a best-fit line through this plot, then, is not affected by system nonlinearity, and therefore the change in nonlinearity can be entirely attributed to the material under investigation.

While longitudinal nonlinear ultrasound has well-documented success in the field of non-destructive evaluation, Rayleigh surface waves are somewhat less established. However, recent work has demonstrated the capability of Rayleigh waves for detecting many of the same microstructural phenomena to which longitudinal NLU is sensitive. In 2006, Herrmann et al. examined low-cycle fatigue and monotonically-loaded nickel-based superalloys using Rayleigh NLU and saw increases in β' of 30-45% and 150-225%, respectively[11]. Liu et al. demonstrated sensitivity in shot-peen Al-7075 samples, which were found to have high levels of residual stress along with cold work as a result of plastic deformation[15]. The combination of these forcings introduced

dislocations and altered the local strain fields, producing increases in the relative acoustic nonlinearity parameter of 20-100%. In 2012, Walker et al. again verified the capability of NLU measurements to detect plastic strain in low-cycle fatigue, reporting roughly a 30% increase in β' for A36 steel plate specimens[24]. Marino et al. extended Cantrell's work on precipitate formation to Rayleigh waves by examining thermal aging of 9% Cr Ferritic Martensitic steel[17]. These measurements indicated a modest net increase of 13% in β' over the course of 3000 hours of artificial aging. In each of these works, the authors indicated the enhanced ability of NLU to accurately detect microstructural changes as compared with traditional, linear ultrasonic methods.

3.5 Applications to Sensitization of 304 Stainless Steel

As mentioned in Chapter 2, a key byproduct of the sensitization process is the formation of chromium carbide precipitates along grain boundaries. These large precipitates form and grow, imposing localized strain fields on the material grains. Sections 3.3 and 3.4 discuss previous work which has demonstrated that the interaction of these precipitate-induced strain fields with dislocation segments increases second harmonic generation within the material, changing the measured acoustic nonlinearity parameter. Furthermore, as discussed in Section 3.4, Rayleigh waves offer several key advantages over longitudinal waves for the purposes of this research. Nonlinear ultrasound using Rayleigh surface waves is therefore a good candidate for detecting the formation of chromium carbide precipitates associated with sensitization in type 304 stainless steel. Chapter 4 will discuss the methods used to generate these waves in a material and extract useful signals from the propagating waves.

CHAPTER IV

EXPERIMENTAL METHODS

The ultimate purpose of using NLU to measure sensitization is to develop a field-ready measurement system capable of evaluating in-situ material properties. By first testing and refining techniques in a laboratory setting, the stage is set for further development of these methods into such a system which will be useful in practical evaluation of structural materials. This chapter describes how a nonlinear ultrasound system uses Rayleigh surface waves to interrogate specimens, and how the data from this interrogation can provide insight into properties of these specimens.

4.1 Experimental Setup

The first step in NLU using Rayleigh waves is to generate the wave packet. An Agilent 33250A 80MHz function generator is used to create the electrical signal. This signal is sinusoidal, with a frequency of 2.1 MHz, amplitude of 800 mV, and length of 30 cycles (0.0143 ms). Each wave packet is generated every 20 milliseconds. After the signal is generated, it passes through a RITEC 2500 gated amplifier. The signal is amplified to 700 V before being sent to the piezoelectric transducer. Piezoelectric transducers are used because they offer consistent, repeatable, and economical conversion between electrical and mechanical waves. A custom Panametrics type X1055 narrow-band transducer with center frequency 2.25 MHz is used for all of the experiments in this research, for reasons discussed in Section 4.3.

The piezoelectric transducer surface generates a mechanical P-wave in direct response to the electrical signal output by the amplifier. This P-wave must be converted into a Rayleigh surface wave, and this is accomplished by employing a plastic wedge. The speed of a Rayleigh wave in 304 stainless steel is computed using Equation (26):

$$c_R = \frac{0.87 + 1.12\nu}{1 + \nu}\sqrt{\frac{G}{\rho}} \tag{26}$$

where ν is Poisson's ratio, G is the shear modulus, and ρ is the material density. Using this value and the measured longitudinal wave velocity in the plastic wedge material, Snell's law is used to calculate the optimal angle for the plastic wedge. θ_w

$$\theta_w = sin^{-1}\frac{c_{D,wedge}}{c_R} \tag{27}$$

This is the angle at which the piezoelectric transducer must be held in order to transform a P-wave in the plastic material into a Rayleigh surface wave in the stainless steel. The transducer is clamped to the rear face of the wedge by means of a custom-made backing plate combined with a pair of screws which can be loosened and tightened to remove, clean, and re-attach the transducer.

After the Rayleigh wave has propagated the desired distance along the material surface, the wave must be detected in order to make observations about the material nonlinearity. In the past, this has often been done using a second, identical plastic wedge and coupled contact transducer. This system works in the same way as on the generation side, in reverse: the Rayleigh wave in the specimen becomes a P-wave in the plastic wedge, propagating at angle θ_w until the wave reaches the receiving contact transducer. However, wedge detection has several disadvantages. Use of a wedge receiver requires that the wedge and transducer be clamped to the specimen surface for each measurement, then unclamped, moved, and re-clamped before moving to the next measurement. This represents a significant time investment for the operator, meaning the method is expensive. Furthermore, it has been shown that these measurements are sensitive to contact conditions — clamping force and amount of oil couplant — making these results somewhat inconsistent[19].

However, re-examination of the wave propagation path demonstrates a useful phenomenon. As the Rayleigh wave packet departs the front face of the wedge and begins

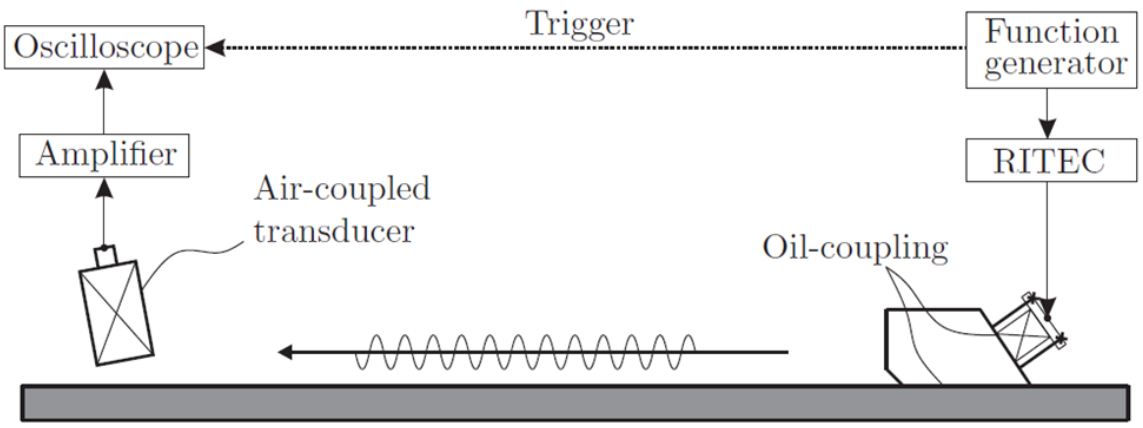

Figure 5: Diagram illustrating the generation, propagation, and detection of a Rayleigh surface wave for NLU measurements[19]

propagating along the surface of the specimen, a "leaked" pressure wave forms in the air adjacent to the surface. This wave forms due to out-of-plane displacement of the surface material as the Rayleigh wave passes through. While this leaked wave carries far less energy than the surface wave, it can be detected using an "air-coupled" transducer, which is sensitive to ultrasonic longitudinal waves in air. This air-coupled detection provides two key advantages over contact measurements. Air-coupled transducers are not in contact with the surface, so they avoid the consistency issues which plague contact conditions. Further, placement of the transducer on a movable (manual or automated) stage allows rapid, highly accurate movement of the transducer to a new location — to adjust the propagation distance of the wave packet, for example.

The electrical signal from the air-coupled receiver travels through an Olympus "Preamplifier", which is used to boost the electrical signal from the transducer without increasing electrical noise. This amplified signal is then funneled into an oscilloscope, where the waveform is captured. A schematic diagram demonstrating the interaction of electrical and mechanical equipment within this setup is shown in Figure 5. At each propagation distance, 512 waveforms are averaged into one time-domain signal which is then run through a post-processing algorithm to compute β'.

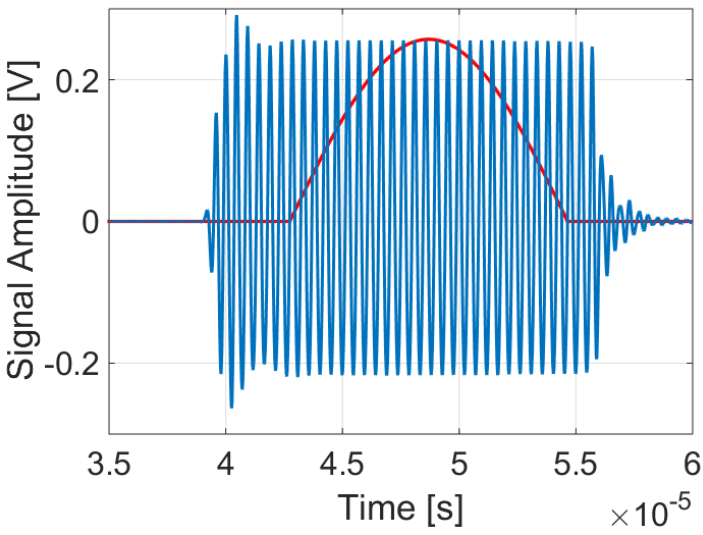

Figure 6: Representative time-domain signal showing 30 cycles of a received Rayleigh surface wave along with an approximate Hann window[14]

4.2 Data Analysis

The data collected from the Rayleigh interrogation is a series of 2-column arrays — one array for each propagation distance at which a measurement is taken. These arrays contain a time vector and 512-sample averaged amplitude vector which, together, represent the time-domain signal. A representative time-domain plot is displayed in Figure 6.

This raw signal is then processed in order to extract useful quantities. If any direct current (DC) offset is present, this is removed first. Any direct component occurs as a result of electrical equipment and is not useful for detecting material nonlinearity. Any interference outside of the window of time during which the wave was detected is also removed in order to ensure that the signal processing algorithm selects peaks only within the desired time envelope.

Peak detection software is then run on the processed signal, and the middle 15 peaks — excluding the first eight and last seven out of 30 total — are identified. The removal of these outer peaks is done to avoid sampling data points affected by

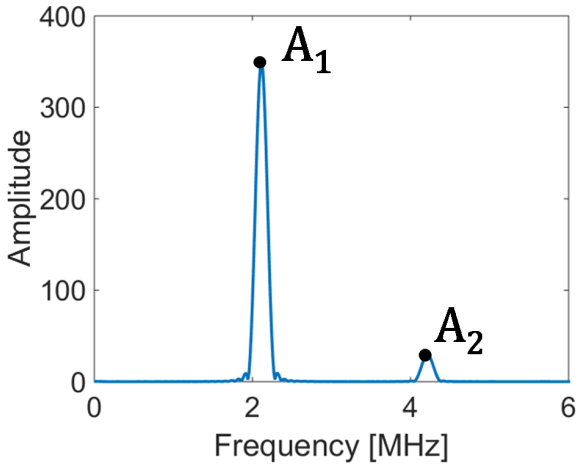

Figure 7: Representative frequency-domain plot with markings indicating A_1 and A_2[14]

transient behavior of either piezoelectric transducer. Selecting the innermost peaks is a reliable way to isolate only steady-state behavior, ignoring electrical effects. A Hann window (shown in Figure 6) is performed on the middle 15 peaks, and this windowed signal is passed through a Fast Fourier Transform (FFT). This mathematical operation identifies constituents of the sinusoidal signal, segregating the component frequencies as demonstrated in Figure 7. The amplitudes of the frequency domain plot at the fundamental and second harmonic frequencies are identified — these quantities represent A_1 and A_2 for the purposes of this research. Plotting the quantity A_2/A_1^2 against propagation distance x gives a set of points which should be roughly linear while A_2 is increasing, although the exact relation is somewhat more complicated[23]. As the phenomenon of interest is second harmonic generation, points beyond the maximum of A_2 are discarded. Finally, a line is fit to the reduced plot, and the slope of this best-fit line is taken as β'.

4.3 Limitations of Current NLU Practices

4.3.1 Calibration of air-coupled transducer

Because the leaked longitudinal wave is much weaker than the Rayleigh surface wave, the air-coupled transducer must be calibrated before being used for measurements. Calibration ensures that the received signal is as high as possible, increasing the signal-to-noise ratio (SNR). This process also locates the propagation axis of the Rayleigh wave packet — the line along which the fundamental frequency component is highest.

First, the optimal angle of the air-coupled transducer is determined. This angle can be computed using simple geometry. Since the leaked pressure wave is generated by out-of-plane displacement of the surface, the angle at which this wave approaches the transducer can be computed using Equation (28):

$$\theta_R = sin^{-1}\frac{c_{D,Air}}{c_{R,SS}} = sin^{-1}\frac{343m/s}{2830m/s} = 6.96^\circ \tag{28}$$

where $c_{D,Air}$ is the longitudinal wave speed in air, $c_{R,SS}$ is the Rayleigh wave speed in stainless steel, and θ_R is the optimal transducer angle measured relative to the surface normal vector (see Figure 5).

Experimental angle calibration is accomplished by creating a set of measurements while holding the transducer at different angles for a constant propagation distance. The measurements are plotted along with a Gaussian fit, and the optimal angle is the x-coordinate of the maximum interpolated A_1. Experimental calibration generally locates the optimal transducer angle between 6.7-7.1°from normal, which agrees with the theoretical value.

The y-coordinate of the propagation axis is then calibrated for both the start and the end of the measurement, as shown in Figure 8. The transducer is placed at the optimal calibrated angle and moved perpendicular to the wedge face while taking incremental measurements at the starting propagation distance. The same procedure

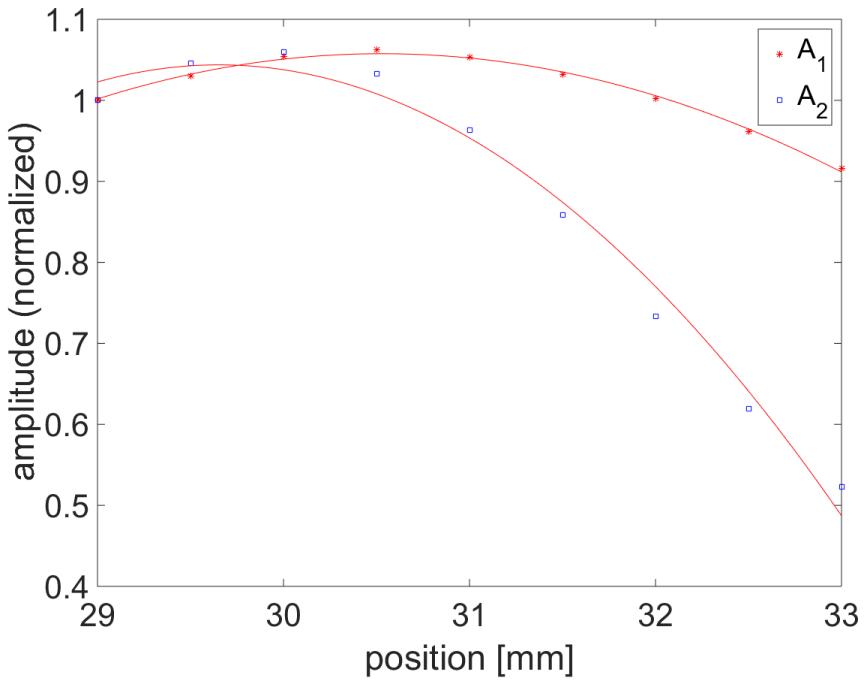

Figure 8: Plot demonstrating the change in A_1 and A_2 with y distance (perpendicular to propagation axis)

is followed for the ending distance, and these two calibration sets are processed and maximum values A_1 extracted. The y-coordinates of these two values represent the location of the maxima fundamental amplitudes at the start and end of the propagation path. Dividing the difference between these coordinates by the number of data points taken for each measurement gives the incremental adjustment necessary to keep the transducer aligned with the propagation path during measurement sets.

Without calibration of the air-coupled transducer, the results obtained from NLU measurements may not be accurate. For example, a perceived increase in second harmonic generation seen in an increasing A_2 may actually be caused by a misaligned transducer crossing into the propagation axis as the transducer is moved in the primary measurement direction. Calibration is therefore essential for air-coupled measurements, a disadvantage as compared with contact NLU measurements.

4.3.2 Relative measurements

A severe limitation of using piezoelectric transducers to generate and receive ultrasonic transducers is that such measurements are inherently relative. The formulation for the acoustic nonlinearity parameter, β, relies on measurement of the absolute fundamental and second harmonic amplitudes A_1 and A_2, respectively. However, piezoelectrics do not measure absolute displacements — rather, each transducer generates and receives signals according to its own unique transfer function, which translates back and forth between mechanical and electrical energies. This means that measurements made on the same specimen but using different transducers may yield vastly different results. Additionally, the use of piezoelectric transducers means that all equipment — wedges, amplifiers, generators, etc. — has an impact on the measured amplitude. For these reasons, the work presented here uses the relative acoustic nonlinearity parameter, β', which is proportional to β as demonstrated in Equation (25) in Section 3.2. This proportionality means that the percentage increase in β' may be compared between experiments and laboratories, but the absolute measurement cannot. Employment of a detection system capable of measuring absolute displacement amplitude, such as a laser interferometer, would yield comparable absolute data, but this work relies solely on relative measurements.

CHAPTER V

OVEN-INDUCED SENSITIZATION

In order to examine sensitization of type 304 stainless steel, it is appropriate to first sensitize specimens using an oven. Oven-induced sensitization introduces few microstructural changes — the uniform process is short enough to avoid thermal aging effects and at a sufficiently low temperature to prevent phase changes. Evading these effects allows the measurement of sensitization alone, permitting the quantification of nonlinearity contribution from the chromium carbide precipitates which accompany the sensitization process. Confirming that NLU is sensitive to oven-induced sensitization is the first step towards in-situ inspection of structures; without this confirmation, any further work with more complicated microstructures is unfounded.

5.1 Theory

The most appropriate formulation for change in nonlinearity with oven-induced sensitization comes from Cantrell's precipitate-matrix misfit model[8]. Derivation of this model is outside the scope of this research, but the governing formulation is described below.

It is assumed that contributions to relative nonlinearity come from the material lattice and dislocations.

$$\Delta\beta' = \Delta\beta^{lat} + \Delta\beta^{disloc} \tag{29}$$

where the lattice contribution is described in Equation (30):

$$\Delta\beta^{lat} = -\frac{B_e}{A_e} \tag{30}$$

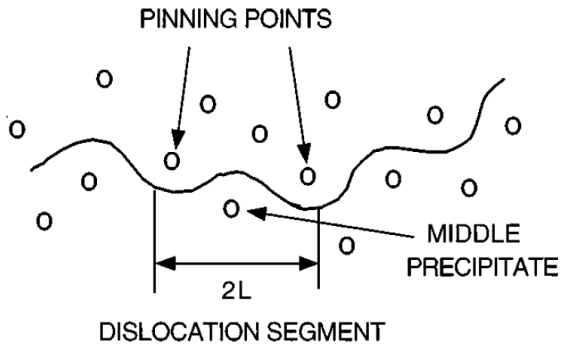

Figure 9: Bowing of dislocation segments in precipitate matrix (from Cantrell et al. 1998[8])

B_e and A_e are the Huang coefficients for the material, and are assumed not to change with oven sensitization. This means the lattice contribution to $\Delta\beta'$ can be neglected, and the change in relative nonlinearity is therefore only dependent on precipitate-dislocation interactions, described in Equation (31):

$$\Delta\beta^{disloc} = \frac{24}{5}\frac{\Omega\Lambda L^4 R^3 \overline{C}_{11}^2}{G^3 b^2}|\overline{\sigma}| \tag{31}$$

where Ω is a conversion factor from shear to longitudinal strain, Λ is the dislocation density, L is half the distance between the dislocation pinning points (as seen in Figure 9), R is the Schmid factor, $\overline{C}_{11}$ is the second-order Brugger elastic constant, G is the shear modulus, b is the Burger's vector, and $\overline{\sigma}$ is the longitudinal stress.

Approximating the longitudinal stress as twice the radial stress in the matrix resulting from a spherical precipitate, and evaluating at half the average distance between two precipitates gives Equation (32):

$$\overline{\sigma} = -\frac{8G(1+\nu)f_p\delta}{3(1-\nu)} \tag{32}$$

Thus, the change in the nonlinearity parameter from precipitate coherency stresses with matrix dislocations is linearly dependent on dislocation density Λ, volume fraction of precipitates f_p, the precipitate-matrix misfit parameter δ, the fourth power of the dislocation loop length L, and common elastic material properties.

Cantrell also related precipitate radius r_p and distance L between two precipitates using Equation (33)[8]:

$$L = \frac{2r_p}{(f_p)^{1/3}} \tag{33}$$

Substituting Equations (32) and (33) into Cantrell's original model gives Equation (34):

$$\Delta\beta^{disloc} = \frac{1024}{5}\frac{\Omega\Lambda r_p^4 R^3 \overline{C}_{11}^2 \delta}{G^2 b^3 (f_p)^{1/3}}\frac{1+\nu}{1-\nu} \tag{34}$$

Most of the terms in this equation will not change with sensitization, whether by thermal treatment or welding. The Schmid factor, material constants, and Burger's vector remain the same, meaning that any increase in acoustic nonlinearity is proportional only to the dislocation density, precipitate radius, and volume fraction of precipitates, as shown in Equation (35):

$$\Delta\beta^{disloc} \propto \frac{\Lambda r_p^4}{(f_p)^{1/3}} \tag{35}$$

This relationship demonstrates extreme sensitivity of the nonlinearity parameter to precipitate radius. Contributions to nonlinearity from dislocation density and volume fraction of precipitates are far lower in comparison, with the effect of volume fraction contributing 12 orders of magnitude less than precipitate radius. Assuming the change in dislocation density is small for oven sensitization, precipitate formation has the only non-negligible contribution to $\Delta\beta'$.

5.2 Background

In 2014, Morlock et al. attempted to measure sensitization and post-cracking SCC specimens using Rayleigh NLU with mixed results[19].

In 2013, Abraham et al. used longitudinal NLU to interrogate oven-sensitized 304 SS[1]. A roughly 60% increase in β' was observed, with little dependence on degree of

sensitization. This indicated that, once sensitized, little difference was seen in β' with increased soaking time, suggesting that the dominant microstructural contribution to nonlinearity came from precipitate formation rather than precipitate growth or dislocation density changes from thermal exposure.

Other measurements of nonlinearity contribution caused by precipitate formation in other materials have yielded more modest increases in β'. Cantrell reported an increase in 8-11% in 2024-Al[8]. Marino et al. saw a net increase of 13% in the nonlinearity parameter using 9%Cr ferritic martensitic steel[17].

5.3 Results

An annealed type 304 stainless steel plate is cut to produce three equally-sized samples (dimensions 6"x2"x3/8" each). These samples are then surface ground and polished to produce a flat, semi-reflective finish. Initial NLU measurements using Rayleigh waves to determine β_0 are made on each specimen using a manually-operated stage.

The three samples are then placed in an oven for two hours at 675°C. This soaking time and temperature has been verified by others to produce sensitization within the material[1, 19]. After two hours, the specimens are removed from the oven and allowed to cool in air. Each sample is then surface ground again to remove scale caused by the treatment. Post-treatment etching and optical microscopy conducted in accordance with ASTM standard A262 indicate the formation of chromium carbide precipitates along grain boundaries. However, full sensitization must be confirmed through observation of ditch microstructures, where carbide precipitates completely surround most grains. As seen in Figure 10, a dual microstructure is present in the treated specimens, indicating only partial sensitization of these three specimens. Post-treatment NLU measurements are taken and compared to the initial readings.

A representative series of plots showing change in A_1, A_2, and β' with x are shown in Figure 11. While A_1 decreases as a result of attenuation and diffraction processes,

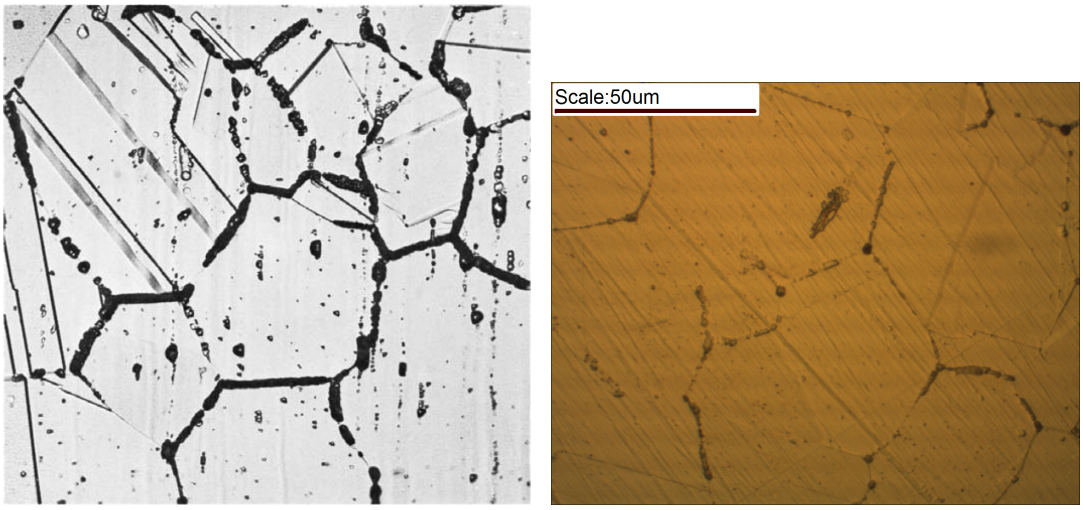

Figure 10: Benchmark "dual" microstructure (left)[3] and micrograph of treated specimen (right)

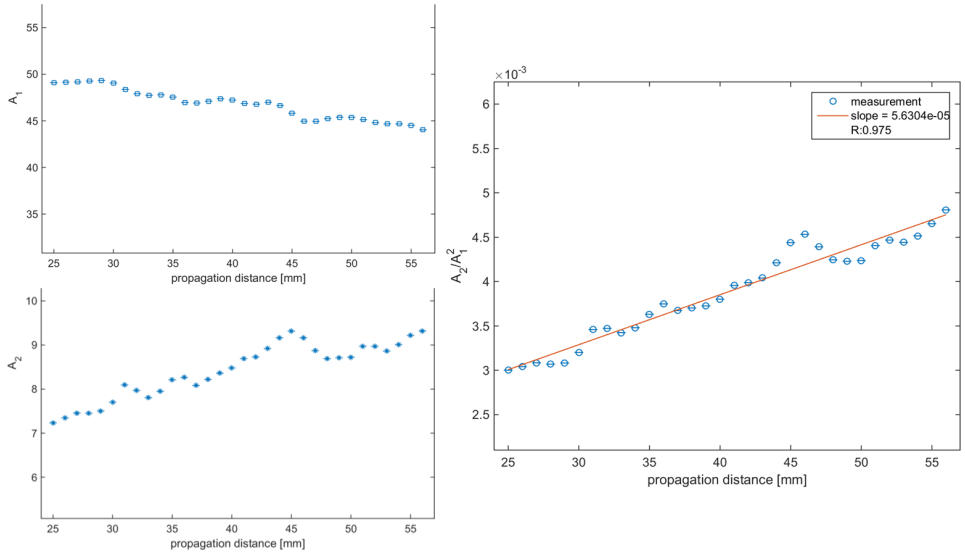

Figure 11: A_1 (top left), A_2 (bottom left), and A_2/A_1^2 (right) versus propagation distance for a representative measurement

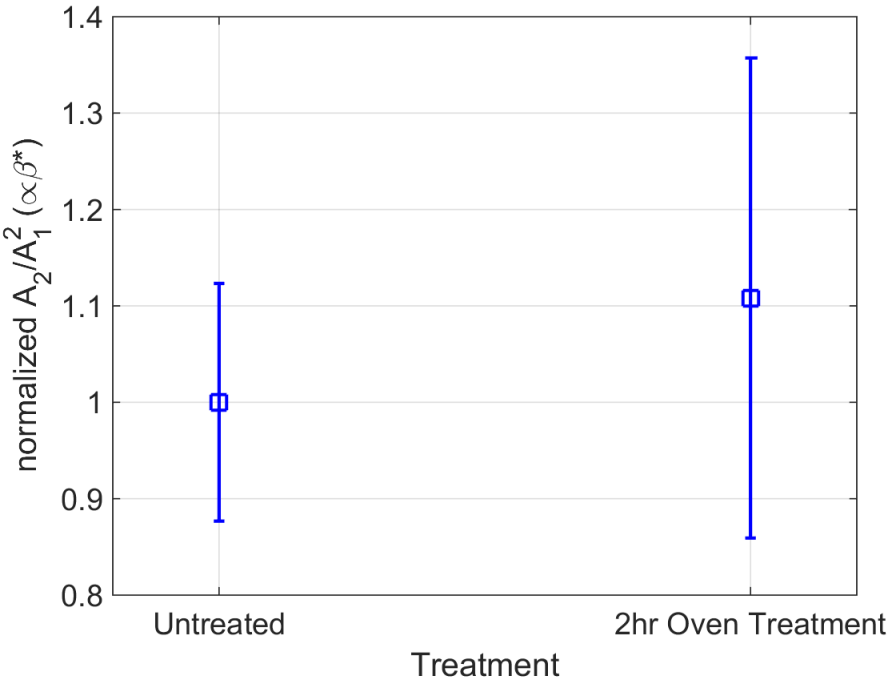

Figure 12: $\Delta\beta'/\beta_0$ before and after oven treatment

A_2 increases with propagation distance due to second harmonic generation. The relationship of β' to x is roughly linear up to the point where A_2 ceases to increase. Based on the second harmonic amplitude plot, all of the data following A_2^{max} is discarded before plotting A_2/A_1^2 against x and performing a linear fit to compute β'. This removal is to ensure that the measurement is only considering effects as the second harmonic generation remains roughly linear, rather than attempting to fit a line to a nonlinear plot[23]. Figure 12 shows the results of the NLU measurements performed, normalized to the average β' prior to treatment.

This result demonstrates that the formation of chromium carbide precipitates within type 304 stainless steel has a measurable effect on nonlinearity, and that NLU using Rayleigh surface waves is sensitive to this microstructural change. Future work, discussed in more detail in Chapter 8, will attempt to fully sensitize the specimens used for this study, providing another data point to verify and compare with ongoing and previous works.

The average increase in β' between the untreated state and post-treatment is 11%. This value is small compared with results obtained by Abraham et al. for the fully-sensitized condition[1]. However, for partial sensitization, this same group reported an increase in β' of 15%, a value which is in good agreement with the current work.

CHAPTER VI

WELD-INDUCED SENSITIZATION

Chapter 5 discusses results concerning stainless steel specimens which have been sensitized via thermal treatment in an oven. While useful for feasibility and sensitivity studies, sensitization in most real-world applications occurs as a result of welding. Empirical observations of stainless steel piping systems indicate that stress corrosion cracking (SCC) typically initiates in the heat-affected zone (HAZ) of a weld. Figure 13 shows a photograph of a pipe fracture resulting from SCC near the welded material.

This portion of the research focuses on the application of NLU methods using Rayleigh waves to detect sensitization caused by welding. Unlike with the oven-induced experiments, welded specimens generally have multiple simultaneous and competing microstructural changes. In addition to the presence of chromium carbide precipitates in welded specimens, there exists a residual stress field as a result of uneven heating and cooling of a welded material. While some work has explored the effect of residual stress on the acoustic nonlinearity parameter, the practice of quantifying a highly localized strain field and determining how the local contributions

Figure 13: Photograph of pipe fracture resulting from stress corrosion cracking near a field weld[10]

impact the measured bulk material second harmonic generation is well beyond the scope of this research. The objective of the present study is to verify that NLU is sensitive to weld-induced sensitization, which would demonstrate feasibility for development of a field-ready method for sensitization detection.

6.1 Theory

As previously mentioned, there are a number of characteristics which complicate weld-induced sensitization microstructure beyond the simple precipitate-dislocation interaction which dominates oven-induced sensitization. Indeed, it is challenging to quantify the competing microstructural changes present in welded samples, and little work has been done thus far to perform NLU measurements within the HAZ region of a weld. This section defines and discusses the expected sources of nonlinearity for such an experiment.

6.1.1 Chromium carbide precipitates

As introduced in Chapter 5, the formation of chromium carbide precipitates is the desired microstructural characteristic for sensitization detection. Equation (35), derived in Section 5.1 from work by Cantrell et al., is reproduced below[8]:

$$\Delta\beta^{disloc} \propto \frac{\Lambda r_p^4}{(f_p)^{1/3}}$$

According to (35), the increase in β' should be proportional to the fourth power of precipitate radius. Even marginally larger chromium carbide precipitates have extreme effects on the measured nonlinearity, and it is possible that the welding process nucleates larger precipitates than does oven treatment. These microstructural effects will be examined and analyzed in future work.

6.1.2 Dislocation density

A major side-effect of sensitization through welding is the introduction of severe and differential localized heating to the material. This process produces significant local plastic strain, imposing a thermal residual stress and introducing dislocations to the crystal structure. Each of these effects has an impact on the measurement of the acoustic nonlinearity parameter.

Dislocation density was first introduced as a contributor to nonlinearity by Hikata et al. in 1965, with further work done by Cantrell[12, 6]). Hikata showed that this nonlinearity results from the displacement of dislocations based on the dislocation density Λ, average loop length $2L$, radius of curvature R, applied stress σ, and material constants as shown in Equation (36):

$$A_2 = A_2^{lat} + \frac{12}{5} \cdot \frac{\Omega E_1^2 L^4 R^3 \Lambda}{\mu^3 b^2} \cdot \sigma \tag{36}$$

This equation indicates that, as with precipitate formation, the contribution to nonlinearity from dislocation density is linear with A_2. Assuming increased dislocation density has little effect on the fundamental amplitude A_1 (a good assumption, as A_1 is not sensitive to nano-scale defects like dislocations), the increase $\Delta\beta'$ seen in the relative acoustic nonlinearity parameter is also linear.

6.1.3 Residual stress

The thermal residual stress introduced to the specimen through uneven heating and cooling also contributes to the material nonlinearity. However, this effect is small for most metals, and will be neglected for the purposes of this research.

Consider the mechanism for second harmonic generation caused by the presence of residual stress. This increased local stress changes the position along the material stress-strain curve. Any second harmonic generation is therefore caused by the

Figure 14: 12"x12"x1" 304 stainless steel plate used for weld sensitization measurements

nonlinearity of the stress-strain relationship (deviation from Hooke's law of elasticity). Since the elastic approximation for stainless steel is very good for stress levels not approaching yield, the contribution to material nonlinearity is small and generally negligible. At residual stresses approaching or exceeding yield, the change in the stress-strain curve is principally due to introduction of dislocation lines and slip planes (accounted for in Section 3.3.1) rather than the presence of residual stress.

The contribution to nonlinearity caused by precipitate formation in the welded specimen is anticipated to be the same or higher than the contribution for the oven-heated specimen. An increase in the dislocation density, which was not seen during the oven treatment, is also expected. The contribution from both of these sources endorses the expectation that measured $\Delta\beta'/\beta_0$ will be higher for weld-induced sensitization than for oven-induced sensitization.

6.2 Results

A large plate (dimensions 12"x12"x1", see Figure 14) composed of type 304 stainless steel is obtained from a material supplier. Along the centerline of the plate, a 5/8" deep, 2" wide, V-shaped notch is cut (see Figure 15). The plate is then clamped at all four corners and welded full with 308 stainless steel filler material. The top

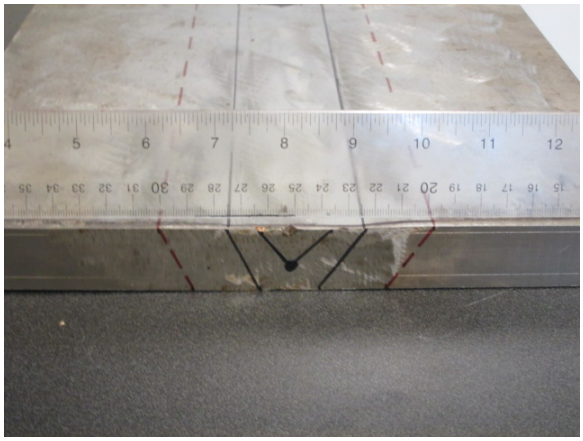

Figure 15: 304 stainless steel weld sensitization plate with edge markings indicating dimensions of notch

and bottom surfaces of the plate are then flattened using a 22" diameter Blanchard grinder, then finished with a cylindrical surface grinder. Both the top and bottom surfaces are then polished using a random orbital sander and sanding block with sandpaper ranging from 50 to 800 grit.

6.2.1 Thermal analysis

In order to estimate the boundaries of the heat-affected zone (HAZ) in this specimen, a rudimentary heat-transfer finite element (FE) model is developed. Output from the model, shown at the bottom of Figure 20, identifies the maximum temperature experienced by each point within the cross section of one (symmetric) half of the plate. According to published work by others, the HAZ in type 304 stainless steel is generally recognized as corresponding to the temperature range of 450-850°C. An estimate of the extents of the HAZ for the plate is superimposed over the model output in the figure.

6.2.2 Nonlinear ultrasound measurements

NLU measurements are made on the welded plate using an air-coupled receiver mounted on an automated scanning stage. The coupled wedge and contact transducer are placed such that the generated Rayleigh wave propagates parallel to the

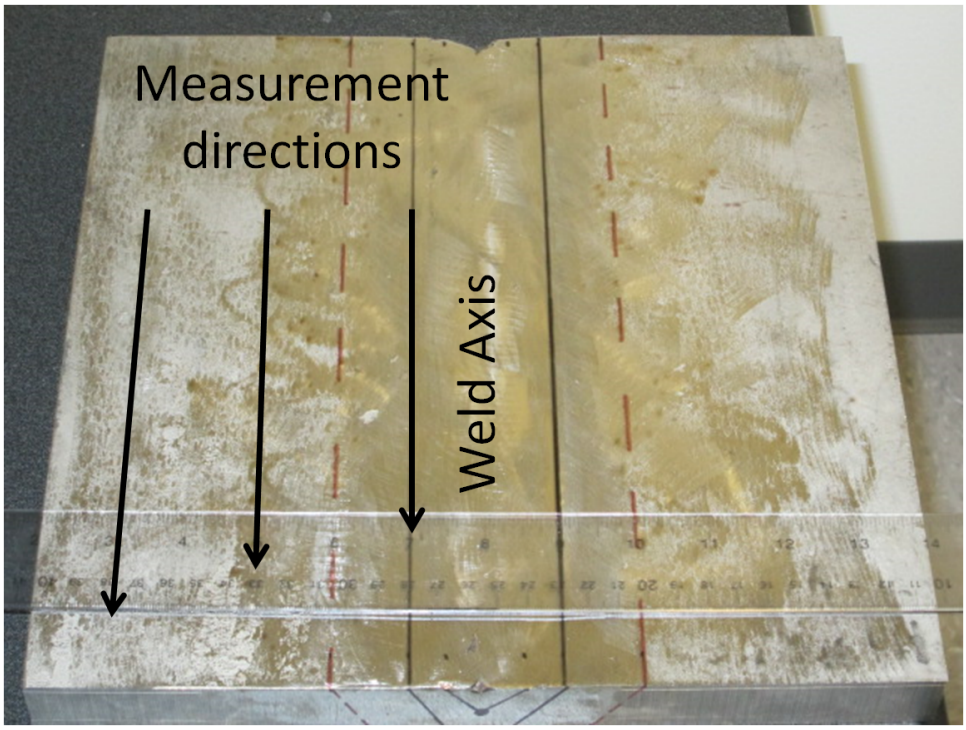

Figure 16: Diagram showing NLU measurements taken parallel to the weld axis

weld axis (see Figure 16). This is done so that the wave will remain in material with approximately the same microstructure throughout the entire propagation distance. Measurements are made spaced in 10mm increments from the weld axis. Three sets of NLU measurements are taken at each incremental location between 20mm and 100mm from the weld axis.

During each measurement, the automated scanner samples along the propagation axis as determined by the calibration process described in Section 4.3.1. Measurements are also taken along lines parallel to the axis, spaced at 0.5mm for 3mm to either side of the propagation axis. Figure 17 plots the fundamental amplitude A_1 for a particular measurement in color, with the x and y axes representing the x and y coordinates of the receiver position relative to the middle of the wedge face. The line y=0 represents the calibrated propagation axis. It is clear from these plots that the fundamental amplitude decreases with propagation distance, as is expected in a material due to attenuation and diffraction losses.

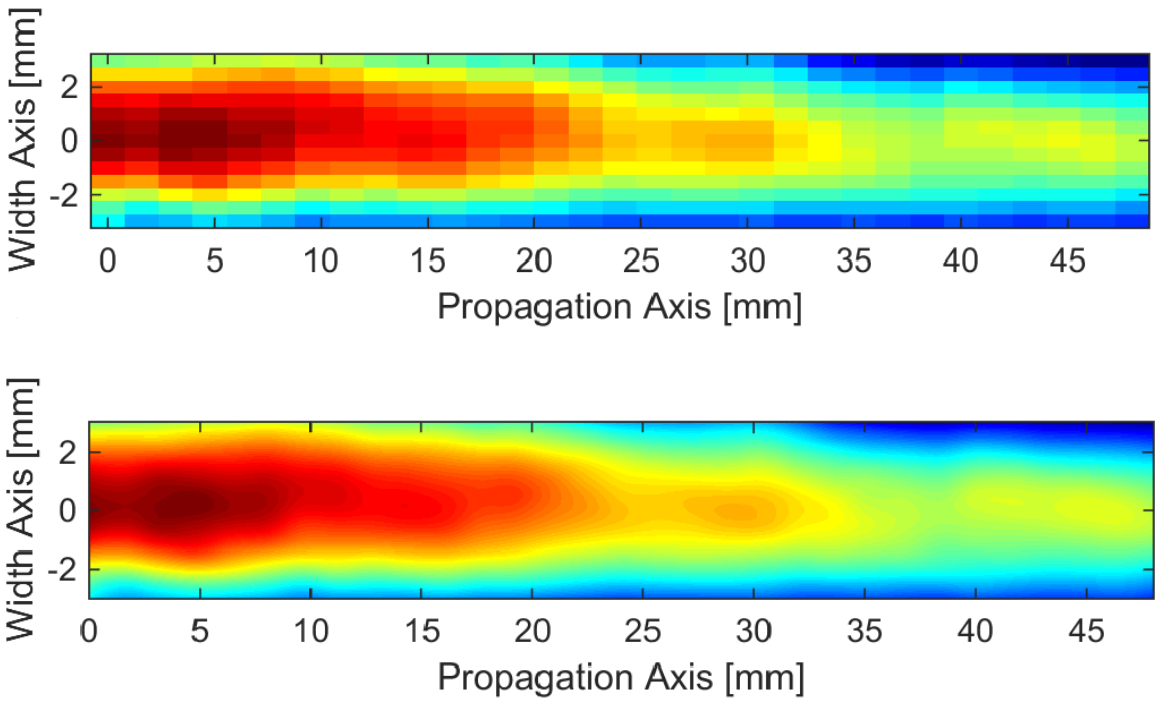

Figure 17: Colormap plots for raw (top) and interpolated (bottom) A_1 for a 2D measurement scan

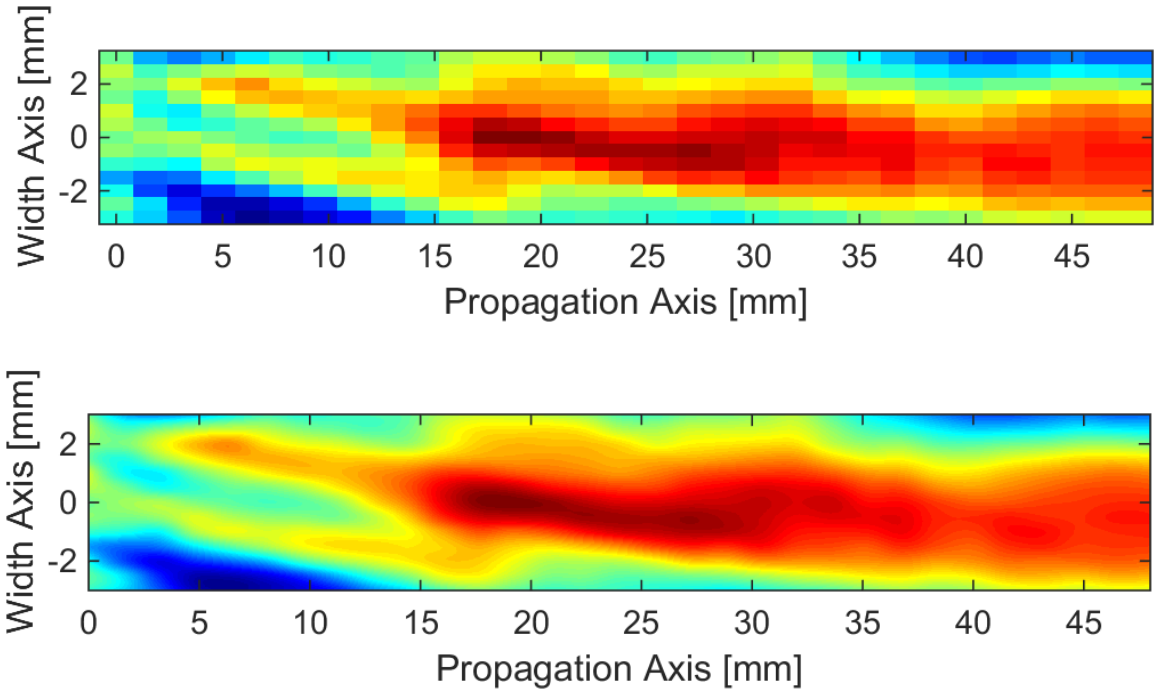

Figure 18: Colormap plots for raw (top) and interpolated (bottom) A_2 for a 2D measurement scan

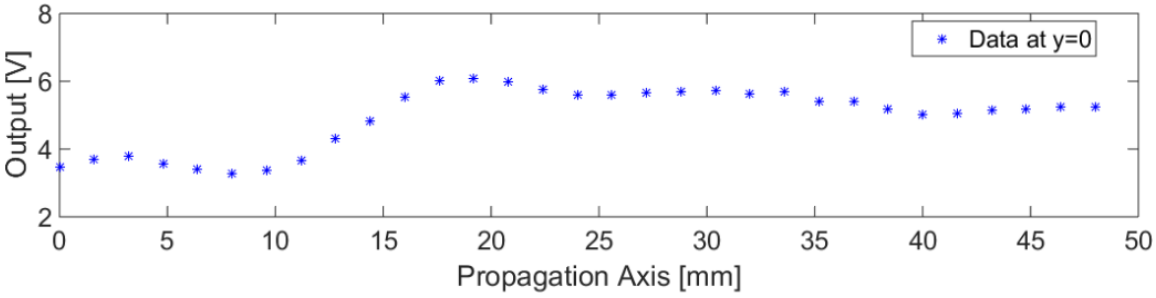

Figure 19: Plot of A_2 with propagation distance along main wave axis

Figure 18 shows the second harmonic amplitude A_2 for the same measurement set. This signal is somewhat less clear, as the signal-to-noise ratio is far lower for A_2 than for A_1. However, it is apparent that the second harmonic amplitude first increases, then decreases with propagation distance along the main axis. This is illustrated in Figure 19. The initial increase is due to second harmonic generation, while the subsequent decrease results as attenuation and diffraction become dominant.

Just as for the oven sensitization results, data points following A_2^{max} are discarded for reasons discussed in Section 5.3 before performing a linear fit of the quantity A_2/A_1^2. After performing this process for all data points collected, the results are summarized in Figure 20 along with the FE model discussed in Section 6.2.1. The x axis of the NLU plot is placed in alignment with the FE model surface such that the tick marks indicating distance from the weld axis correspond to the physical distance from the weld axis on the model output.

One data point, taken at 20mm from the weld axis, is omitted here as it was found to be within the fusion zone of the weld and therefore irrelevant to the current research. The results in Figure 20 demonstrate a clear increase in β' near the HAZ of the weld. There appears to be a clear separation between measurements taken "far" from the weld and those taken within the HAZ. Averaging the data points within each of these respective groups, β' within the HAZ is 223% greater than "far" from the weld.

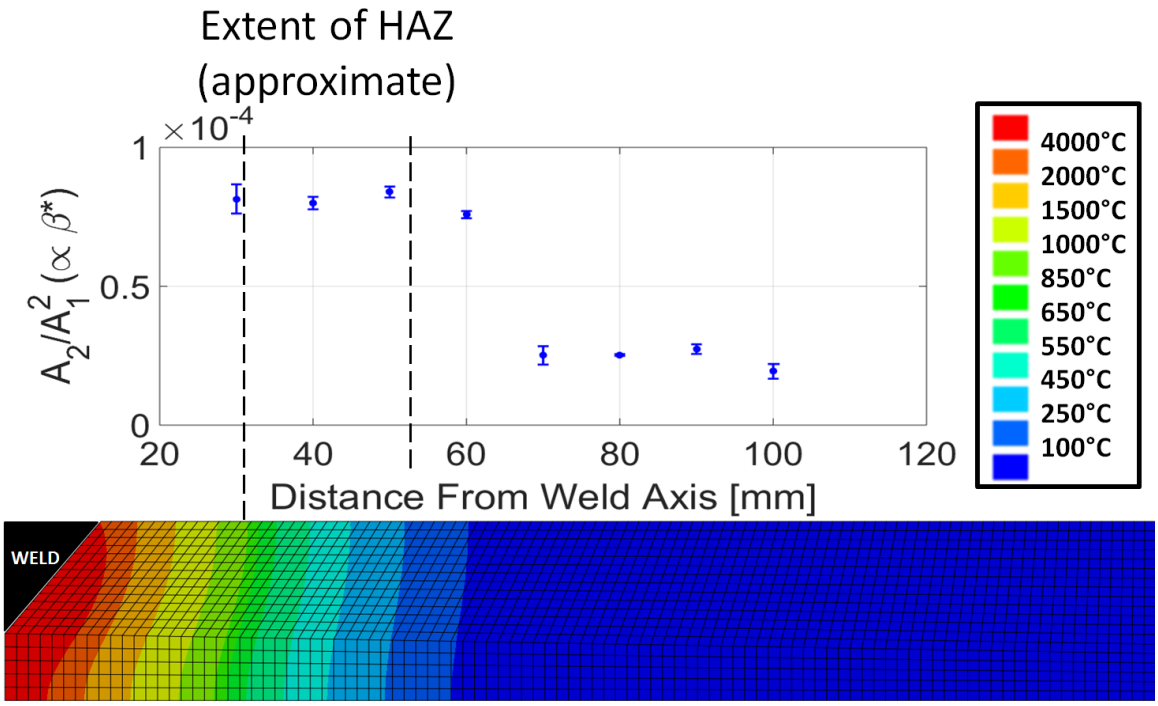

Figure 20: Nonlinear ultrasound results superimposed above heat-transfer FE model output showing approximate maximum temperature at each point during welding

It was anticipated that dislocation density would increase somewhat as measurements approached the high heat region of the weld, and that this microstructure would result in higher values of β'. However, there does not appear to be significant variation between measurements made within the HAZ. One explanation is that the dislocation density is not great enough to have a measureable effect on the nonlinearity for this specimen. This could also be a sign that the sharp increase in β' is caused by formation of precipitates with extraordinarily large radii in the HAZ, which dominate the nonlinear response and overshadow any contribution from increased dislocation density.

6.2.3 Comparison to oven-induced sensitization

This section discusses how results from NLU of oven-induced sensitization (Chapter 5) differ from those of weld-induced sensitization (Chapter 6). As discussed in the respective chapters, β' increases within partially sensitized oven specimens by 11%

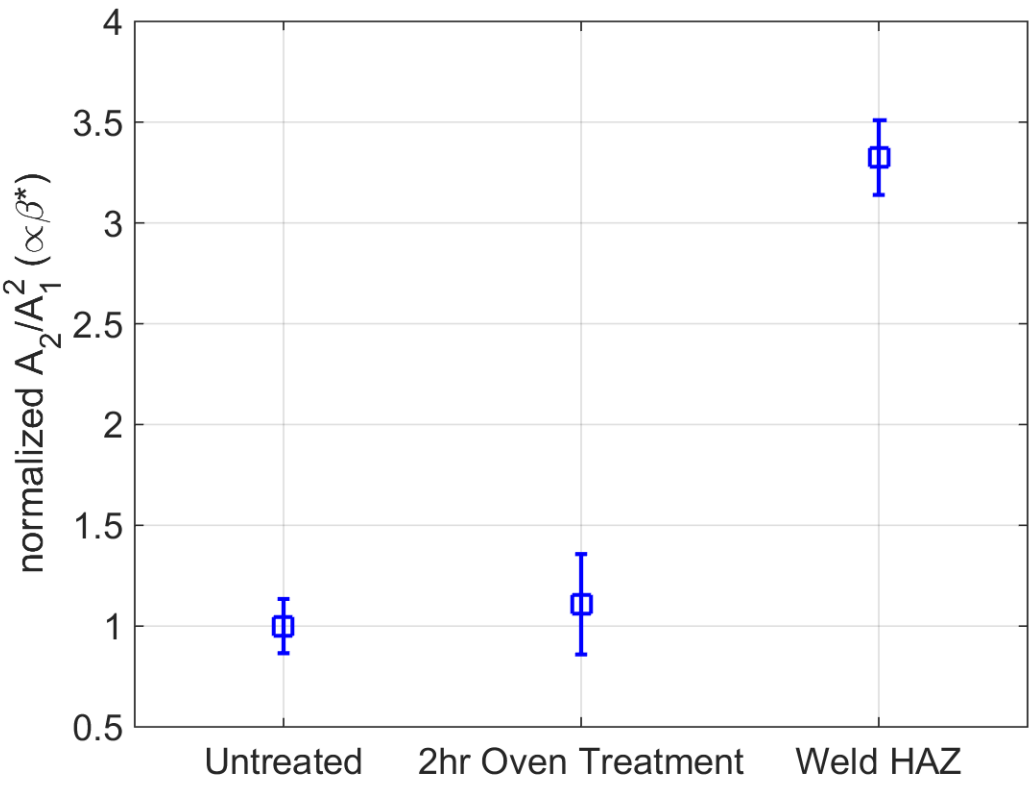

Figure 21: Comparison of $\Delta\beta'/\beta_0$ for partial oven sensitization and weld HAZ measurements

and in the HAZ of the welded specimen by 223%. Figure 21 shows these two results in comparison to the untreated state (note that the untreated data point includes measurements made both on oven specimens prior to treatment and on the welded specimen far from the weld axis). As expected, the variance in measurements increases for the partial oven sensitization and weld HAZ measurements. This is most likely due to the nature of relative measurements — as microstructural nonlinearities increase, measurements become more sensitive to localized changes.

It is likely that the additional nonlinearity seen in weld-induced sensitization results from either precipitates which have larger radii than those created by thermal treatment, or interaction of similar-sized precipitates with a more dense dislocation network. Future work, examined in Chapter 8 will attempt to determine which of

these two phenomena is responsible for the significant increase in β'.

CHAPTER VII

CONCLUSIONS

This research examines the use of nonlinear ultrasound (NLU) with the second harmonic generation technique to detect microstructural changes resulting from sensitization in type 304 stainless steel. Rayleigh waves are generated using a coupled piezoelectric transducer and plastic wedge. Use of an air-coupled receiver provides simplified measurements, offering low contact variance and isolation of the desired quantity — material nonlinearity. Based on the electrical signal output from the receiver at the fundamental and second harmonic frequencies, the relative acoustic nonlinearity parameter is computed.

Previous work has used both Rayleigh and longitudinal NLU to examine precipitate formation in a variety of materials, including at least two papers dealing with sensitization in 304 stainless steel. The goals of this work are to verify the capability of nonlinear Rayleigh waves to detect sensitization resulting from a standard oven treatment and to investigate whether sensitization in the heat-affected zone (HAZ) of a weld can be identified using the same method — something which has not been done with a non-destructive evaluation technique previously. Initial "base" readings are taken on untreated samples of stainless steel. These specimens are then subjected to 2 hours of treatment in an oven at 675°C in order to induce sensitization. Subsequently, microscopy is conducted, verifying the formation of chromium carbide precipitates and confirming the onset of partial sensitization. Comparison of NLU readings after the treatment indicates an increase in the relative acoustic nonlinearity parameter of 11%, a value which compares well to previous work in detection of microstructural changes associated with precipitate formation.

A large stainless steel plate is welded along the centerline. Far from the weld, the material is assumed to retain its "as-received" properties and measurements made at this location can therefore provide the base readings for this sample. Successive measurements are made, remaining parallel to, while moving closer to, the weld axis. The hypothesis that material nonlinearity increases with decreasing proximity to the weld is confirmed, although readings within the heat-affected zone appear relatively insensitive to distance from the weld axis. The nonlinearity parameter shows a sharp increase of 223% at the boundary between the far field and the HAZ. Interaction of several competing microstructural processes is examined and discussed.

CHAPTER VIII

FUTURE WORK

The most immediate future work will involve attempts to fully sensitize the oven-induced specimens discussed in Chapter 5. While examining partial sensitization is both interesting and useful in providing a data point for comparison with other work, fully sensitized microstructures are of greater interest to industries dealing with stress corrosion cracking of structural materials. After further sensitization, the specimens will be re-evaluated using Rayleigh NLU.

While NLU results from the HAZ of the welded stainless steel plate (Chapter 6) are promising, more work needs to be done for the results to be verified. Because of the complicated series of microstructural changes present within this region, destructive evaluation techniques will be indispensable to substantiate the data presented here. Such examination can provide insight into the nature of sensitization within this region, answering questions about why measured nonlinearity is so much greater in the HAZ than in the oven-induced sensitization samples.

A final more significant and long-term goal will be to begin making absolute measurements of the true acoustic nonlinearity parameter. Thus far, much of the work done in the field of NLU has been relative, involving transmitted and received electrical signals using piezoelectric transducers. Each transducer has its own transfer function based on the center frequency and individual mechanical characteristics, meaning that such transducers are incapable of directly measuring the surface displacement or velocity in the presence of a propagating wave. This problem can be solved through the use of a powerful laser interferometer capable of sensing the higher harmonic amplitudes of ultrasonic waves. Alternatively, individual transducers can

be calibrated by comparison with an absolute measurement system in order to retain the useful traits of piezoelectrics without sacrificing detection ability.

REFERENCES

[1] Abraham, S. T., Albert, S. K., Das, C. R., Parvathavarthini, N., Venkatraman, B., Mini, R. S., and Balasubramaniam, K., "Assessment of sensitization in AISI 304 stainless steel by nonlinear ultrasonic method," *Acta Metallurgica Sinica (English Letters)*, vol. 26, no. 5, pp. 545–552, 2013.

[2] ASCE, "2013 Report Card for America's Infrastructure - Bridges," tech. rep., American Society of Civil Engineers, 2013.

[3] ASTM International, "A262: Standard Practices for Detecting Susceptibility to Intergranular Attack in Austenitic Stainless Steels," tech. rep., 2014.

[4] Bedford, A. and Drumheller, D. S., *Introduction to elastic wave propagation*. 1994.

[5] Callister Jr., W. D., *Materials Science and Engineering: An Introduction*. Hoboken, NJ: John Wiley & Sons, Inc., 7 ed., 2007.

[6] Cantrell, J. H., *Fundamentals and Applications of Nonlinear Ultrasonic Nondestructive Evaluation*. CRC Press LLC, 2004.

[7] Cantrell, J. H. and Yost, W. T., "Nonlinear ultrasonic characterization of fatigue microstructures," *International Journal of Fatigue*, vol. 23, no. 1, pp. 487–490, 2001.

[8] Cantrell, J. H. and Zhang, X.-G., "Nonlinear acoustic response from precipitate-matrix misfit in a dislocation network," *Journal of Applied Physics*, vol. 84, no. 10, p. 5469, 1998.

[9] Contreras, A., Salazar, M., Albiter, A., Galvan, R., and Vega, O., "Assessment of Stress Corrosion Cracking on Pipeline Steels Weldments Used in the Petroleum Industry by Slow Strain Rate Tests," in *Arc Welding*, ch. Assessment, pp. 127–150, InTech, 2011.

[10] DGZfP, "Abstracts of the Annual DGZfP Conference," (Dresden), 1997.

[11] Herrmann, J., Kim, J.-Y., Jacobs, L. J., Qu, J., Littles, J. W., and Savage, M. F., "Assessment of material damage in a nickel-base superalloy using nonlinear Rayleigh surface waves," *Journal of Applied Physics*, vol. 99, no. 12, p. 124913, 2006.

[12] Hikata, A., Chick, B. B., and Elbaum, C., "Dislocation contribution to the second harmonic generation of ultrasonic waves," *Journal of Applied Physics*, vol. 36, no. 1965, pp. 229–236, 1965.

[13] Hurley, D. C., Balzar, D., Purtscher, P. T., and Hollman, K. W., "Nonlinear ultrasonic parameter in quenched martensitic steels," *Journal of Applied Physics*, vol. 83, no. 9, p. 4584, 1998.

[14] Lakocy, A. J., Kim, J.-y., Wall, J. J., and Jacobs, L. J., "Experimental Characterization of Sensitization in Stainless Steel using Nonlinear Rayleigh Waves - QNDE Conference 2015," 2015.

[15] Liu, M., Kim, J.-Y., Jacobs, L., and Qu, J., "Experimental study of nonlinear Rayleigh wave propagation in shot-peened aluminum plates," *NDT & E International*, vol. 44, no. 1, pp. 67–74, 2010.

[16] Marino, D., *Using nonlinear ultrasound measurements to assess the stage of thermal damage in modified 9% CR ferritic martensitic steel*. MS thesis, 2014.

[17] Marino, D., Kim, J.-Y., Ruiz, A., Joo, Y.-s., Qu, J., and Jacobs, L. J., "Using Nonlinear Ultrasound to Track Microstructural Changes due to Thermal Aging in Modified 9%Cr Ferritic Martensitic Steel," *NDT & E International*, 2015.

[18] Matweb, A. S. M., "AISI Type 304 Stainless Steel."

[19] Morlock, F., *Evaluation of stress corrosion cracking in sensitized 304 stainless steel using nonlinear Rayleigh waves*. MS thesis, 2014.

[20] Schweitzer, P. A., *METALLIC MATERIALS: Physical, Mechanical, and Corrosion Properties*. Marcel Dekker, Inc., 2003.

[21] Shui, Y. and Solodov, I. Y., "Nonlinear properties of Rayleigh and Stoneley waves in solids," *Journal of Applied Physics*, vol. 64, no. 11, p. 6155, 1988.

[22] Torello, D., "Transducer Calibration," 2015.

[23] Torello, D., Thiele, S., Matlack, K. H., Kim, J.-Y., Qu, J., and Jacobs, L. J., "Diffraction, attenuation, and source corrections for nonlinear Rayleigh wave ultrasonic measurements," *Ultrasonics*, vol. 56, no. September, pp. 417–426, 2015.

[24] Walker, S. V., Kim, J.-Y., Qu, J., and Jacobs, L. J., "Fatigue damage evaluation in A36 steel using nonlinear Rayleigh surface waves," *NDT & E International*, vol. 48, pp. 10–15, 2012.